Rationalizing Nanomaterial Sizes Measured by Atomic Force Microscopy, Flow Field-Flow Fractionation, and Dynamic Light Scattering: Sample Preparation, Polydispersity, and Particle...

ARTICLE *in* ENVIRONMENTAL SCIENCE & TECHNOLOGY · MAY 2012

Impact Factor: 5.33 · DOI: 10.1021/es301167x · Source: PubMed

2 AUTHORS, INCLUDING:

Mohammed Baalousha
University of South Carolina
51 PUBLICATIONS **2,168** CITATIONS

SEE PROFILE

Environmental Science & Technology

Article

pubs.acs.org/est

Rationalizing Nanomaterial Sizes Measured by Atomic Force Microscopy, Flow Field-Flow Fractionation, and Dynamic Light Scattering: Sample Preparation, Polydispersity, and Particle Structure

M. Baalousha* and J. R. Lead

School of Geography, Earth and Environmental Sciences, College of Life and Environmental Sciences, University of Birmingham, Edgbaston, Birmingham B15 2TT, United Kingdom

Supporting Information

ABSTRACT: This study aims to rationalize the variability in the measured size of nanomaterials (NMs) by some of the most commonly applied techniques in the field of nano(eco)toxicology and environmental sciences, including atomic force microscopy (AFM), dynamic light scattering (DLS), and flow field-flow fractionation (FlFFF). A validated sample preparation procedure for size evaluation by AFM is presented, along with a quantitative explanation of the variability of measured sizes by FlFFF, AFM, and DLS. The ratio of the *z*-average hydrodynamic diameter (d_{DLS}) by DLS and the particle height by AFM (d_{AFM}) approaches 1.0 for monodisperse samples and increases with sample polydispersity. A polydispersity index of 0.1 is suggested as a suitable limit above which DLS data can no longer be interpreted accurately. Conversion of the volume particle size distribution (PSD) by FlFFF–UV to the number PSD reduces the differences observed between the sizes measured by FlFFF (d_{FlFFF}) and AFM. The remaining differences in the measured sizes can be attributed to particle structure (sphericity and permeability). The ratio d_{FlFFF}/d_{AFM} approaches 1 for small ion-coated NMs, which can be described as hard spheres, whereas d_{FlFFF}/d_{AFM} deviates from 1 for polymer-coated NMs, indicating that these particles are permeable, nonspherical, or both. These findings improve our understanding of the rather scattered data on NM size measurements reported in the environmental and nano(eco)toxicology literature and provide a tool for comparison of the measured sizes by different techniques.

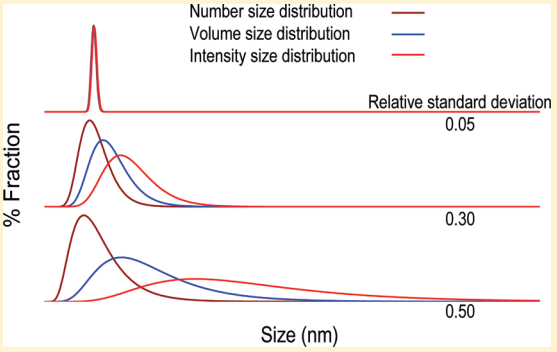

INTRODUCTION

Nanotechnology is a rapidly growing industry which is expected to play a leading role in shaping the future of manufacturing processes and consumer products. Estimates suggest that the global market for nanoenabled industry is expected to be worth over $2.41 trillion by 2015.[1] The number of consumer products apparently containing nanomaterials (NMs) has grown rapidly in the past decade and is projected to increase even more rapidly in the future.[2] Many of the applications of these novel materials will bring considerable benefits and improvements in the quality of life. However, the small size of NMs (1–100 nm)[3] means that they may have unique and different biouptake and toxicity mechanisms compared with ionic counterparts.[4,5] To study biological uptake and effects, transport, and exposure of chemicals in a reproducible manner, consistent and accurate measurement of their chemical composition and physical structure must be performed reliably. In the case of NMs, particle size distributions (PSDs) and other properties might influence the biological effects and need to be determined accurately.[6] Clearly, there is a lack of certainty about NM interactions with biological and environmental systems and a lack of understanding of the structure–property (toxicity) relationships.[7,8] In terms of structure, the lack of understanding results mainly from the lack of physicochemical metrology and characterization of NMs, the absence of validated procedures for sample preparation, and the difficulty in interpreting data obtained by different analytical tools.[9,10] Several studies have reported large variability between the sizes measured by the different techniques and related this to differences in the distribution weighing, the measurement principle, the measured parameters, or the aggregation state of the sample.[9,10] However, such studies were performed on nonstandard, commercially available NMs, making interpretation difficult.[9,11,12] Those studies have therefore suggested the need for in-depth characterization of well-controlled NMs and a multimethod approach to quantify their properties.[9,11−13] However, characterization of NM physicochemical properties using a multimethod approach is not always feasible, as the required analytical tools are rarely available in the same research

Received: March 26, 2012
Revised: May 15, 2012
Accepted: May 17, 2012
Published: May 17, 2012

   dx.doi.org/10.1021/es301167x | Environ. Sci. Technol. 2012, 46, 6134–6142

institute, require extensive expertise, and have associated large infrastructure and running costs.[9] Nonetheless, application of a single technique might lead to erroneous conclusions being drawn, unless any variability between the results can be rationalized. The application of such data to environmental and (eoc)toxicological research stems from the need to accurately quantify particle properties to understand their environmental and biological behavior.

In this study we aim to identify, rationalize, and reduce the sources of variability of the sizes measured by three commonly used analytical tools. Atomic force microscopy (AFM) provides a physical measurement of particle size (height) and provides a number-weighted PSD. Flow field-flow fractionation (FlFFF) and dynamic light scattering (DLS) measure the diffusion coefficient of particles from which a hydrodynamic diameter can be calculated and provide mass- and intensity-weighted size distributions and averages, respectively. Well-stabilized suspensions including a range of commercially available and in-house synthesized NMs were selected to avoid any variability induced by processes such as aggregation and dissolution of NMs during analysis. Emphasis was given to (i) sample preparation to develop standardized protocols that will reduce analysis variability, (ii) sample polydispersity as all NM suspensions have a certain level of polydispersity which influences size measurement, and (iii) NM structure (sphericity and permeability) by comparing the size measured by FlFFF, DLS, and AFM.

This study provides a tool for comparison of the measured sizes by different analytical tools and, therefore, improves our understanding of the rather scattered data on NM size measurements reported in the environmental and nano(eco)-toxicology literature.

MATERIALS AND METHODS

Commercially Available Nanomaterial Standards. Two sets of NMs have been used in this study. The first is a set of three sizes of citrate-stabilized gold NM standards, nominally 10, 30, and 60 nm (National Institute of Standards and Technology (NIST), Gaithersburg, MD). The second is a set of four NIST traceable size standards of polystyrene NMs, nominally 20, 30, 40, and 59 nm, with a narrow standard deviation (Thermo Scientific, United Kingdom). The certified sizes of these standards are summarized in the Supporting Information (Table S1).

In-House-Synthesized Nanomaterials. Citrate-stabilized gold (citrate−AuNM1 and citrate−AuNM2) and silver (citrate−AgNM1 and citrate−AgNM2) NMs as well as poly(*N*-vinyl-2-pyrrolidone) (PVP)-stabilized gold (PVP−AuNM1 and PVP−AuNM2) and silver (PVP−AgNM1 and PVP−AgNM2) NMs were synthesized in-house to study the effect of the nature of the surface coating on the NM structure (sphericity and permeability). More details of the synthesis methods can be found in the Supporting Information and references therein.[14]

Atomic Force Microscopy. Different sample preparation techniques were employed for particle analysis by AFM, including adsorption from solution, sorption from a thin layer, drop deposition, and ultracentrifugation,[15−18] to verify the effect of sample preparation on the measured sizes. For each sample, about 100−160 height measurements on individual NMs (aggregates were not accounted for to avoid aggregation artifacts) were performed from randomly selected areas of the slide, and the measured heights were classified into intervals of 1−2 nm. Different distribution functions, including Gaussian, Lorentzian, and log-normal distributions,[19,20] were used to model the measured size distributions, from which an average particle size (d_{AFM}) and standard deviation were calculated. More details about AFM analysis are provided in the Supporting Information).

Field-Flow Fractionation. Separation and sizing of NMs were performed in an asymmetrical flow field-flow fractionation. The correlation between the polystyrene standard (20, 30, 40, and 59 nm) retention time and size was used as a calibration curve to convert the elution fractograms into a PSD, from which the average particle size (d_{FlFFF}) and the standard deviation were calculated. More details about FlFFF analysis are provided in the Supporting Information.

Dynamic Light Scattering. DLS constructs an autocorrelation function from the measured fluctuations in the scattered light intensity over time. This autocorrelation function decays exponentially as a function of the correlator time delay, and this in turn is a function of the particle diffusion coefficient. The equivalent hydrodynamic diameter of the particles can be determined from the diffusion coefficient by applying the Stokes−Einstein relationship, which assumes that particles are spherical and hard (nonpermeable).[21,22] The Malvern DLS instrument uses two methods to analyze the autocorrelation function: (i) cumulant analysis (gives a *z*-average hydrodynamic diameter (d_{DLS}) and a measure of the sample polydispersity, which is the polydispersity index, PDI) and (ii) distribution analysis (gives an intensity-weighted size distribution). The outcome of these methods and how they compare to AFM measurements are investigated in detail in the Results and Discussion. More details of the DLS data analysis are provided in the Supporting Information.

RESULTS AND DISCUSSION

Validation of Sample Preparation for AFM Analysis. Sample preparation for AFM analysis requires fixation of the sample (NMs) to a substrate, and this can impact the results considerably (e.g., by producing artifacts of drying or sample overloading). Here we optimize the sample preparation for particle sizing using AFM by comparing different sample preparation methods that have been used in the literature without any validation with reference nanoparticles of accurately known sizes.[23,24] These sample preparation methods include adsorption from solution, adsorption from a thin layer, drop deposition, and ultracentrifugation.[16,17] The sample preparation methods were compared using a set of polystyrene and gold-certified reference NMs of well-known sizes.

For the sorption from solution method, only small NMs (i.e., 20 nm polystyrene and 10 nm gold NMs, Figure S1A, Supporting Information) were observed, whereas larger polystyrene and gold NMs were not observed at all. For all other methods (sorption from a thin layer, drop deposition, and ultracentrifugation), some NMs of all samples were detected and measured by AFM. For the drop deposition method, typical aggregation artifacts due to drying effects were observed (Figure S2A, Supporting Informaiton), but these artifacts were not observed for other sample preparation methods, and therefore, the heights of individual NMs were considered for statistical analysis. For ultracentrifugation, sample overloading (Figure S2B) was observed at high concentrations (generally >1 mg L^{-1}), and these samples were discarded and prepared at lower concentrations (i.e., <1 mg L^{-1}). At these concentrations, ultracentrifugation shows homogeneously distributed NPs on

dx.doi.org/10.1021/es301167x | Environ. Sci. Technol. 2012, 46, 6134−6142

Table 1. Average Sizes (nm) Measured by AFM Using Different Sample Preparations[a]

	sorption from solution for 30 min	drop deposition	sorption from a thin layer/drop on the mica for 30 min	centrifugation at 150000*g* for 60 min
LB 20 nm	14.7 ± 8.3 (0.56)[b]	NA	NA	15.5 ± 3.6 (0.23)[b]
	176			100
LB 30 nm	ND[c]	13.4 ± 7.50 (0.56)	24.5 ± 6.30 (0.26)[b]	24.7 ± 4.1 (0.17)[b]
		100	123	104
LB 40 nm	ND[c]	26.9 ± 9.00 (0.34)	31.0 ± 10.4 (0.34)	37.6 ± 7.80 (0.21)
		105	112	107
LB 60 nm	ND[c]	30.0 ± 11.1 (0.37)	60.1 ± 10.4 (0.17)[b]	63.3 ± 8.80 (0.14)[b]
		106	120	103
Au 10 nm	8.1 ± 1.7 (0.21)	NA	7.20 ± 1.50 (0.21)	9.60 ± 1.20 (0.16)
	122		125	100
Au 30 nm	ND	NA	15.8 ± 6.30 (0.40)	29.5 ± 2.40 (0.08)
			111	120
Au 60 nm	ND	NA	<30 nm	58.3 ± 4.40 (0.08)
			50	105

[a]All sizes were measured on individual particles only (aggregates were not accounted for to avoid aggregation artifacts), are reported as the mean ± standard deviation (relative standard deviation). The second line is the number of particles measured and used to calculate the particle size distribution, average, standard deviation, and relative standard deviation. NA = samples were not analyzed. ND = particles were not detected. [b]Means are not significantly different. Otherwise, for entries not marked with a superscript "*b*", the means are significantly different. [c]Sorption from solution for 24 h was also performed in addition to sorption for 30 min.

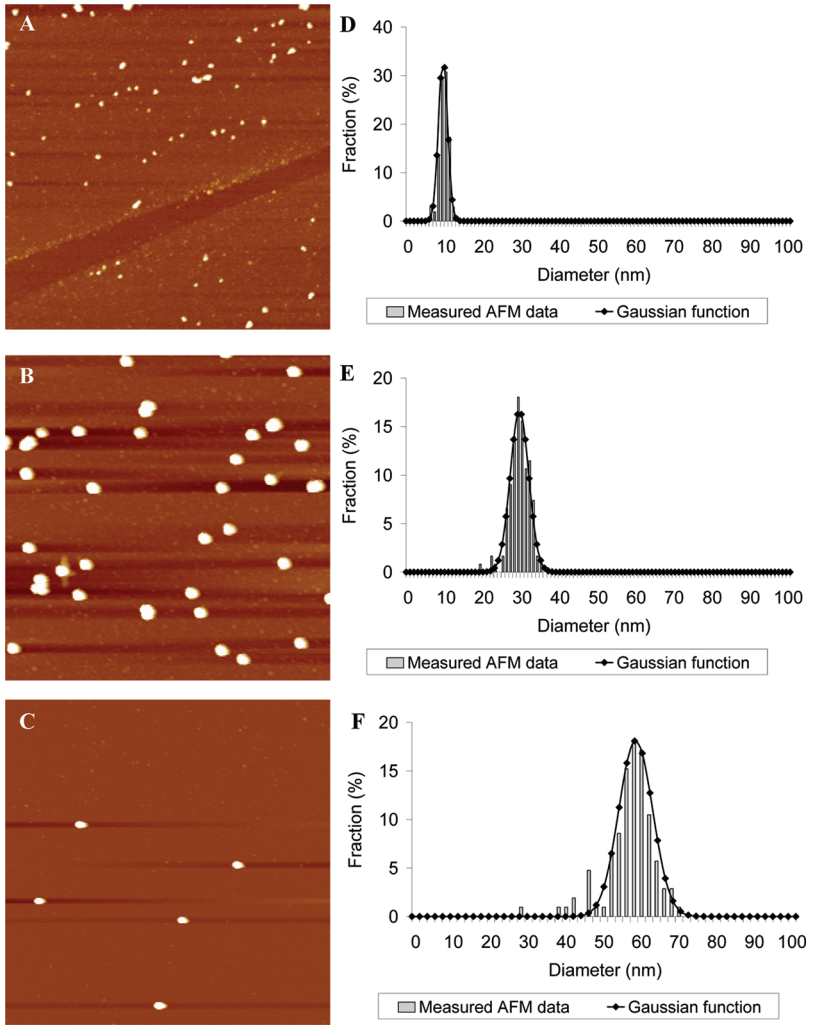

Figure 1. Typical AFM micrographs of NIST Au NMs prepared by the ultracentrifugation (150000*g* for 60 min) method: (A) 10 nm, 2 × 2 μm, (B) 30 nm, 2 × 2 μm, (C) 60 nm, 5 × 5 μm.

dx.doi.org/10.1021/es301167x | *Environ. Sci. Technol.* 2012, 46, 6134–6142

the mica substrate (Figure 1). It is worth noting that the low concentration required for the ultracentrifugation method makes it a method of choice to study NMs at environmentally relevant concentrations. For highly concentrated samples, either sample dilution (as discussed above) or the centrifugation of smaller volumes allows substrate overloading artifacts to be overcome.

Figure S1 (Supporting Information) shows a comparison of typical AFM images obtained on a AuNM standard (NIST 8011, 10 nm) prepared using the sorption from solution, sorption from a thin layer, and ultracentrifugation methods. For the same sample concentration (0.26 μg of Au L^{-1}), very few NMs are observed on the mica surface when samples are prepared by sorption methods, whereas a larger number of NMs are observed when samples are prepared using the ultracentrifugation method.

More quantitatively, the average sizes calculated from samples prepared by these methods are summarized in Table 1. The following observations can be made: (i) the ultracentrifugation method provides the most accurate particle sizes compared to the certified values for the polystyrene and gold NM standards, (ii) the sorption method provides accurate sizes for only the small sizes (20 nm polystyrene and 10 nm gold NMs), (iii) the drop deposition method generally underestimates the size of the particles, and (iv) the sorption from a thin layer provides accurate measurements for the polystyrene NMs, whereas it underestimates the size of the gold NMs.

Sorption is a passive method and depends largely on the nature of the surface (e.g., charge of the substrate and the NMs), as well as on particle diffusion to the substrate surface, and therefore is biased toward small NMs and those NMs that can interact strongly with the substrate. The drop deposition method is known to induce aggregation artifacts due to locally increased salt concentrations on drying,[25,26] hence the aggregation artifacts observed in Figure S2A (Supporting Information). In contrast, the centrifugation method is an active method that allows recovery of the whole number of particles within the suspension onto the mica surface and therefore provides the best measurement of the NM size. Therefore, on the basis of these data, ultracentrifugation is the most appropriate sample preparation method providing the most representative size distribution as demonstrated for the set of polystyrene and gold NM standards and requires diluted samples (<1 mg L^{-1}). This conclusion is consistent with our previous work on sample preparation for transmission electron microscopy (TEM) applying ultracentrifugation commercially available NMs.[11,12] Consequently, all AFM analyses of the in-house-synthesized AuNMs and AgNMs were only performed on samples prepared by ultracentrifugation, and AFM images of all samples together with the measured PSDs are presented in Figure S4 (Supporting Information). Generally, all samples have narrow PSDs, except three samples (PVP−AgNM1 (Figure S4H) and PVP−AuNM1 and PVP−AuNM2 (data not shown here)), which have wider PSDs.

The number of particles required to obtain the statistically representative mean particle size and standard deviation of the entire population of NMs depends on the sample polydispersity and varies in the range of 80−120 nanoparticles for NMs investigated in this study (see the discussion and Figure S3 in the Supporting Information). However, a larger number of particles may be required for higher polydispersity NMs.[27] Furthermore, to minimize any artifacts due to measuring a relatively small number (100−160 per sample) of NMs by AFM, different distribution functions, including Gaussian, Lorentzian, and log-normal distributions,[19,20] were used to model the measured PSD and to calculate the number-average size and standard deviation. Most samples were best fitted by a Gaussian distribution function, except three samples (PVP−AuNM1, PVP−AuNM2, and PVP−AgNM1), which were best fitted by a log-normal distribution function due to their relatively high polydispersity compared to the other samples (see the discussion, Table S2,a nd Figure S4 in the Supporting Information).

Optimization of Measurement by DLS. Table S3 (Supporting Information) shows the sizes measured by DLS of the polystyrene and gold standards and shows relatively good agreement between the measured and the certified *z*-average hydrodynamic diameters (Table S1, Supporting Information). However, conversion of the measured intensity distribution to number and volume distributions results in underestimation of the calculated number and volume averages (Tables S3 and S4) in comparison to the certified and measured sizes by AFM (Tables S1 and S2), and this underestimation is even more significant for the general purpose (GP) analysis algorithm (Table S3). The multiple narrow peak (MNP) algorithm shows a better fit of the autocorrelation function (Figure S6A, Supporting Information) and closer estimation of the number-average particle size (Table S4) compared to the certified values and those measured by AFM (Tables S1 and S2). Furthermore, increasing the number of intervals used for distribution analysis by DLS to 100−300 intervals results in an improved fit (Figure S6A) and a better estimate of the number-average sizes compared to the certified sizes (Table S1) and to AFM number averages (Table S2).

The distribution analysis by DLS is dependent on the parameters used to fit the data, including the number of intervals and the lower and upper size limits. The default parameters set up by the manufacturer (Malvern 70 intervals, 0.4 and 10 000 nm, respectively) do not always provide the best fitting and consequently do not provide the most representative particle sizes and size distributions and therefore should not be used routinely. Optimizing the DLS distribution analysis affects the shape of the intensity-weighted size distribution histogram (Figure S6B, Supporting Information), which will have significant consequences for the conversion to number and volume size distributions as shown in Figure S6C,D (see also Tables S3−S5, Supporting Information, for comparison of the calculated sizes). The GP model provides the least accurate fitting (Figure S6A) and therefore the least accurate size distribution analysis. It provides a broad intensity size distribution that results in distortion of the calculated volume and number size distribution and a shift toward smaller sizes (Figure S6). The MNP algorithm provides a better fit, which improves further at a higher number of size intervals (Figure S6A). The intensity, volume, and number averages obtained using the MNP algorithm are much closer to each other and to the *z*-average hydrodynamic diameters (Table S4) compared to those obtained using the GP algorithm (Table S3). Therefore, for distribution analysis, the selection of the model (GP vs MNP) and the fitting parameters (number of intervals and others that were not considered here due to the limited access to the DLS data and data analysis software) is crucial to obtain the most representative PSD. The intensity particle size distribution obtained by DLS depends on the applied analysis algorithm. The GP model should not be used even for monodisperse samples.

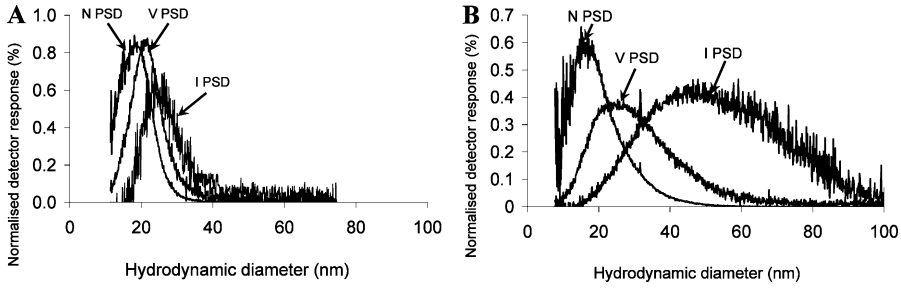

Figure 2. Typical FlFFF fractograms of two samples representing (A) a monodisperse sample, PVP−AgNMs2, and (B) a polydisperse sample, PVP−AgNM1. N PSD is the number particle size distribution calculated as previously described in the main text. V PSD is the volume particle size distribution obtained from the UV absorption at a wavelength of 400 nm, specific for silver. I PSD is the intensity particle size distribution obtained from the scattered light intensity collected at a 90° angle.

It is worth noting that intensity PSD conversion to a number/volume PSD should be performed carefully as the presence of a small amount of scattering from small molecules (free PVP, for instance) will skew the data toward a smaller number/volume PSD, which dominates the distributions (Figure S7A, Supporting Information), and in such a case, data conversion should only be performed after the removal of light scattering (e.g., by data processing) from these small molecules (Figure S7B).

Optimization of FlFFF Calibration. Sample overloading, due to a high NM concentration, results in a shift of the particle peak toward smaller elution volume and therefore underestimation of the measured sizes. Here, initial investigation of a possible overloading effect[28] was performed systematically on the studied NMs by performing NM separation at a range of concentrations (data not shown), and no overloading effect was observed for all samples at concentrations of 1−5 mg L^{-1} with a 500 μL injection volume. Only fractograms with no overloading effects were converted to PSDs and used to calculate particle sizes.

FlFFF theory can be applied to calculate the diffusion coefficient and the equivalent hydrodynamic diameter distribution of NMs, directly from their retention time and the channel dimensions. In some literature data, the channel volume (and thickness) was usually determined by measuring the "void time" or "breakthrough time" of very small or very large macromolecules/particles with the cross-flow turned off.[29,30] However, the accumulation wall membrane is flexible, and the channel thickness can be expected to depend on both cross-flow and the carrier liquid composition. Therefore, a preferred method is the calibration of the channel thickness by a series of spherical standard NMs covering the range of NM sizes being separated using the same flow rates and carrier composition as the sample, without changing the carrier after the analysis of the sample.[28] This method provides a linear relationship between elution time and particle size (Figure S5, Supporting Information), which can then be used to determine the size of unknown particles. However, such a calibration is dependent on the NMs used as size standards. So far polystyrene nanospheres have been used routinely to calibrate FlFFF.[28] However, these polystyrene nanospheres have been certified only for the z average or number average by techniques different from FlFFF. For instance, the 20, 30, and 40 nm polystyrene NMs used in this study were standardized for the z-average hydrodynamic diameter by DLS, whereas the 60 nm NM was standardized for the number-average diameter by TEM. It is therefore not clear that using the certified standard diameters is optimal. The standardization of NM sizes using different instrumentation makes it difficult to generate any useful calibrations for FlFFF due to differences in average weightings. This can only be overcome by (i) using a sizing technique that provides a volume size distribution for certification of standards to be used for FlFFF calibration, (ii) converting the measured PSD (number by microscopy techniques or intensity by DLS) on these particles to a volume PSD, or (iii) using highly monodisperse (i.e., relative standard deviation (RSD; σ_d/d) <0.1) standard NPs, but such standards are not yet available.

Figure S5 (Supporting Information) shows the calibration curve of FlFFF using both the z-average diameter and the calculated volume average from the number distributions measured by AFM and suggests that using NMs which have been standardized for the z average to calibrate FlFFF may result in ∼5−10% overestimation of the particle size. This suggests that for instrumental calibration the appropriate weighted size average should be used, that is, a volume-average diameter for the FlFFF−UV method rather than a z-average hydrodynamic diameter, for which the polystyrene beads are standardized.

Figure 2 shows the separation of PVP-coated silver NMs by FlFFF detected by UV and light scattering (LS). The UV data were converted into a number particle size distribution as discussed elsewhere.[31] Clearly, sample PVP−AgNM2 has a narrow particle size distribution and a small shift among the number-, volume-, and intensity-weighted distributions. However, sample PVP−AgNMs1 shows a rather more polydisperse sample with a broader particle size distribution and a significant shift among the number-, volume-, and intensity-weighted particle size distributions. The number-, volume-, and intensity-average sizes calculated from FlFFF−UV−LS fractograms are 18.5 ± 4.4, 21.7 ± 4.8, and 32.4 ± 11.8 nm for PVP−AgNM2 and 19.8 ± 8.1, 27.5 ± 7.0, and 56.1 ± 20.3 for PVP−AgNM1. This example clearly illustrates that the increase in particle polydispersity results in an increased shift among the number, volume, and intensity particle size distributions. This in turn will inevitably result in data misinterpretation and misunderstanding and overestimation of the particle size if LS is used as the detector. Nonetheless, LS can be very useful for the detection of larger particles (and aggregates of particles). The higher polydispersity of sample PVP−AgNM1 compared to PVP−AgNM2 can be attributed to the differences in the synthesis methods (see the Supporting Information, synthesis of silver NMs). These observations are in good agreement with AFM observations discussed above and presented in Figure S4 (Supporting Information). The number and volume averages of all NMs are summarized in Table 2 and the Supporting

Table 2. Summary of Nanoparticle Sizes (nm) Measured by FlFFF, AFM, and DLS[a]

	V_{av} d_{FlFFF} ± σ_d (σ_d/d)	N_{av} d_{FlFFF} ± σ_d	d_{AFM} ± σ_d (σ_d/d)	d_{DLS} ± σ_r (PDI)	d_{DLS}/d_{AFM}	d_{DLS}/V_{av} d_{FlFFF}	V_{av} d_{FlFFF}/d_{AFM}	N_{av} d_{FlFFF}/d_{AFM}	t (nm) = N_{av} d_{FlFFF} − d_{AFM}
LB 20 ± 2 nm			15.5 ± 3.6 (0.23)	21.0 ± 0.07 (0.09)	1.44				
LB 30 ± 1 nm			24.7 ± 4.1 (0.17)	30.3 ± 0.09 (0.07)	1.22				
LB 40 ± 1 nm			37.6 ± 7.8 (0.21)	40.6 ± 0.06 (0.06)	1.17				
LB 59 ± 2 nm			63.3 ± 8.8 (0.14)	63.5 ± 0.2 (0.006)	1.00				
Au 10 nm	12.2 ± 4.6 (0.37)	9.30 ± 2.6	9.60 ± 1.2 (0.13)	14.0 ± 0.4 (0.27)	1.54	1.15	1.27	0.97	
Au 30 nm	35.5 ± 6.5 (0.18)	32.8 ± 5.2	29.5 ± 2.4 (0.08)	28.2 ± 0.3 (0.160)	0.98	0.80	1.20	1.11	1.65
Au 60 nm			58.3 ± 4.4 (0.08)	55.5 ± 0.2 (0.100)	0.99				
citrate−AuNM1	11.8 ± 4.4 (0.37)	8.30 ± 3.1	7.80 ± 2.3 (0.29)	17.6 ± 0.4 (0.44)	2.29	1.50	1.51	1.06	0.25
citrate−AuNM2	16.0 ± 5.0 (0.31)	14.4 ± 3.0	13.3 ± 1.3 (0.10)	20.6 ± 0.5 (0.29)	1.61	1.29	1.20	1.08	0.55
PVP−Au NM1	19.7 ± 14.5 (0.74)	6.0 ± 3.3[b]	10.4 ± 4.9 (0.47)	32.2 ± 0.5 (0.49)	3.25	1.63	1.89	1.36	3.00
			13.7 ± 4.9 (0.36)[b]						
PVP−AuNM2	19.5 ± 7.5 (0.38)	15.3 ± 4.4	9.50 ± 3.5 (0.37)	21.7 ± 0.8 (0.31)	2.13	1.11	2.05	1.61	2.9
citrate−AgNM1	12.7 ± 3.5 (0.28)	10.6 ± 2.6	10.8 ± 4.0 (0.37)				1.18	0.98	
citrate−AgNM2	7.5 ± 2.5 (0.33)	6.30 ± 1.5	6.70 ± 3.1 (0.46)				1.12	0.94	
PVP−AgNM1	27.5 ± 8.1 (0.29)	19.8 ± 7.0	12.0 ± 4.3 (0.36)	31.6 ± 0.2 (0.47)	2.82	1.15	2.29	1.65	3.9
PVP−AgNM2	21.7 ± 4.8 (0.22)	18.5 ± 4.4	11.5 ± 2.6 (0.23)	21.4 ± 0.2 (0.30)	1.83	0.99	1.89	1.61	3.5

[a] V_{av} = volume average. N_{av} = number average. d_{FlFFF} = hydrodynamic diameter measured by FlFFF. d_{DLS} = z-average hydrodynamic diameter measured by DLS. d_{AFM} = number-average diameter measured by AFM. t = estimated surface coating thickness (nm). σ_r represents the repeatability of the measurement (the ability to achieve the same measurement consecutively). σ_d represents the standard deviation about the mean of all particles counted in a sample. σ_d/d = RSD. [b] Volume to number gave an erroneous conversion; hence, the AFM number distribution was converted to a volume distribution for this sample to calculate d_{FlFFF}/d_{AFM}.

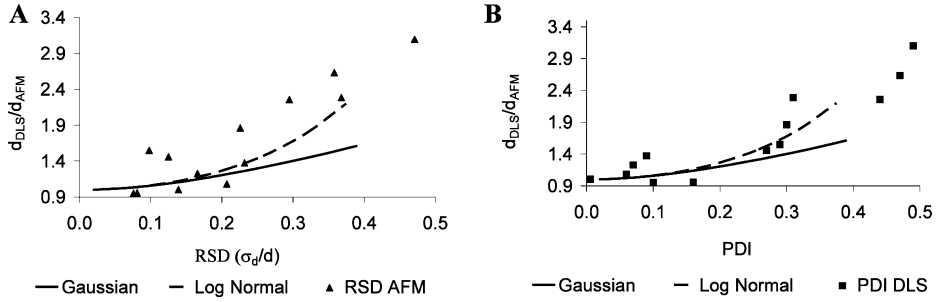

Figure 3. Correlation between sample polydispersity indices (A, relative standard deviation (RSD) measured by AFM; B, polydispersity (PDI) measured by DLS) and the ratio between the z-average hydrodynamic diameter measured by DLS (d_{DLS}) and number-average particle size measured by AFM (d_{AFM}). The dashed curves are the theoretical relationships between the relative standard deviation and the intensity-average/number-average diameters (for more details, see the Supporting Information).

Information (Table S2). All NMs have small RSDs, except three samples (PVP−AuNM1, PVP−AuNM2, and PVP−AgNM1; Table 2).

Variability in Measured Sizes. When considered collectively, the particle sizes measured by AFM, DLS, and FlFFF (Table 2) suggest that the raw average sizes obtained by different methods (number average, volume average, and z average) are generally different except for some samples (Au 30 nm and Au 60 nm). The explanation is that different analytical techniques provide different measurements of particle size, as they are based on different principles.[9,10] The differences in the measured sizes may lead to different sizes or size distributions reported for the same particles. This will lead to biased outputs where a single technique rather than a multimethod approach is relied upon.[9,11,12] However, a systematic investigation of the differences of the measured sizes can provide additional information on sources of variability in the measured sizes, as well as general rules for reporting measured sizes. Here, we investigate the variability among d_{AFM}, d_{DLS}, and d_{FlFFF} in relation to (i) weighting of the PSD, (ii) the polydispersity of the samples, and (iii) the structure of the particles.

AFM vs DLS. Figure 3 shows the correlation between the measured polydispersity indices (RSD by AFM and PDI by DLS) and d_{DLS}/d_{AFM}. It is clear that d_{DLS}/d_{AFM} varies within the range of 0.95−3.1, approaches 1.0 for low PDI values (monodisperse samples), and increases with the sample

dx.doi.org/10.1021/es301167x | Environ. Sci. Technol. 2012, 46, 6134−6142

polydispersity. Therefore, the difference between d_{DLS} and d_{AFM} has been attributed to the sample polydispersity and structure (see the discussion below). Thus, as expected, d_{DLS} is the least accurate/representative size measurement for these NMs in polydisperse samples resulting from the presence of a small fraction of larger sizes of NMs that scatter more light than the small NMs that dominate the sample by number or mass concentration as AFM and FlFFF data suggest. The results suggest that DLS is of very limited use for accurate particle sizing of "real" samples and provides accurate results only for highly monodisperse samples (i.e., PDI < 0.1). Any deviation in particle polydispersity will result in a large deviation of d_{DLS} from the true particle size. It is therefore clear that AFM and DLS will only produce similar results for monodisperse samples (i.e., PDI by DLS and RSD by AFM <0.1). This is in good agreement with the theoretical calculations presented in Figure 3 (dashed curves; for more more details see the Supporting Information). The larger d_{DLS}/d_{AFM} ratio compared to the theoretical curves (Figure 3) is likely to be related to the NM structure (discussed below) or to the presence of a small fraction of larger materials that result in overestimation of d_{DLS}. Due to the lack of accuracy of the conversion of the intensity PSD obtained by DLS to a number PSD and the dependence of the calculated number PSD on the fitting parameters (see discussion above), comparison of the number PSD by DLS and number PSD by AFM was not performed here.

FlFFF vs DLS. The ratio d_{DLS}/V_{av} d_{FlFFF} varies within the range of 0.80−1.63 (Table 2) and again increases with tan increase in the PDI by DLS and the RSD by FlFFF, confirming the findings of the previous section. However, direct comparison between the sizes measured by DLS and FlFFF requires the conversion of the z average to volume average, which is not sufficiently accurate as discussed in the previous section.

AFM vs FlFFF. The ratio V_{av} d_{FlFFF}/d_{AFM} varies within the range of 1.18−2.29 (Table 2) and again increases with an increase in the RSD by FlFFF and AFM. Nonetheless, the variability in the measured sizes by the different techniques can be minimized by converting the obtained size distributions to the same weighted size distribution as demonstrated previously for sizes measured by FlFFF and AFM.[31] Conversion from a higher order (volume) to a lower order (number) PSD was found to reduce the conversion error compared to the reverse conversion (number to volume)[31] and is therefore recommended for any PSD conversion calculations. The ratio between the number averages calculated from FlFFF (N_{av} d_{FlFFF}) and AFM (d_{AFM}) (0.94−1.65, Table 2) shows better agreement between calculated sizes than the ratio V_{av} d_{FlFFF}/d_{AFM}. In addition, N_{av} d_{FlFFF}/d_{AFM} is about 0.94−1.11 for small ion (citrate) stabilized NMs and 1.36−1.65 for large polymer (PVP) stabilized NMs, suggesting a structural difference between the particles rather than an analytical error. Most likely, the higher ratios are due to the softness or permeability of the polymer and the failure of the Stokes−Einstein relationship for these types of materials. This interpretation is in agreement with our previous analysis for natural organic macromolecules[31] and for iron oxide.[32] From these data, citrate-coated NMs may be considered as hard spheres, whereas PVP-coated NMs behave as soft, permeable particles, where the core Ag or gold is spherical, but the geometry of the polymer coating is as yet undetermined. It is worth noting that reported trends should be considered carefully when dealing with multipopulation of particle sizes. Additionally, the differences between appropriately converted data for FlFFF and AFM can provide an estimate of the thickness of the surface coating (Table 2), and this varies within 0−0.55 nm for citrate-coated NMs to 1.65−3.9 nm for PVP-coated NMs.

Recommendations. There are a variety of analytical tools that can be used for the determination of NM size which quite often provide different values of particle size for the same sample under consideration, hence the common recommendation in the recent literature of the need for a multimethod approach for NM characterization.[9,11−13] While physicochemical characterization of NMs by a multimethod approach is a plausible option, a better understanding of the sources of variability between the analytical techniques could simplify the task and provide a tool for the scientific community to correlate particle sizes measured by different techniques (in different research groups). In this paper we have addressed the sources of variability of the measured sizes by three commonly used analytical techniques (AFM, DLS, and FlFFF). Our findings suggest that the raw sizes (e.g., number, by AFM, mass/volume, by FlFFF, and intensity, by DLS, average particle sizes) are only comparable for highly monodisperse hard spheres. Nonetheless, the variability in raw sizes by different analytical techniques can be rationalized by considering (i) sample preparation, (ii) PSD weighing, (iii) particle polydispersity, and (iv) particle structure. The following recommendations are made when reporting the NM size and size distribution to allow for rational comparison between the measured sizes. These recommendations can also be applied for other size characterization techniques.

(i) Sample preparation should be considered carefully (and reported fully) to ensure the representativeness of the entire sample. For AFM analysis, the ultracentrifugation method is generally optimal for manufactured NMs, although there is a need to optimize the sample concentration/volume to avoid artifacts due to sample overloading. For FlFFF, the use of calibration standards has been addressed, and we recommend the use of standards calibrated for the volume average when using UV as a detector. Additionally, optimal experimental parameters should be chosen, primarily flow rates and use of low mass concentrations, to reduce channel overloading, particle−particle interactions, and particle−membrane interactions as discussed elsewhere.[28] For DLS, the quality of the fitting of the autocorrelation function is key in obtaining the correct measure of particle size, that is, z-average hydrodynamic diameter by cumulant analysis or intensity-weighted size distribution by distribution analysis.

(ii) There should be a fully transparent reporting of the size and size distribution by different techniques. Indeed, it is preferable to report a size distribution, although a measure of sample polydispersity together with the measured average size might be sufficient. For instance, the z-average hydrodynamic diameter should be reported together with the PDI, and the number-average diameter by AFM and volume-average diameter by FlFFF should be reported together with the (relative) standard deviation of the distribution.

(iii) Conversion of sizes to the same distribution weighting (i.e., intensity, mass, or number) is the ideal way to compare sizes measured by different techniques. PSD should be converted from higher order to lower order

weighting (i.e., from intensity to mass to number) to reduce calculation error.[31] If the conversion of the PSD is not accurate such as in the case of converting the DLS intensity PSD to the number-average PSD, indices of polydispersity such as the PDI index by DLS and the RSD by AFM (Figure 3) can be used as a guiding rule for comparison of sizes measured by different techniques. In all cases, comparison of sizes measured by different techniques should be made while keeping in mind the sources of variability between the measured sizes, such as sample polydispersity and particle structure.

(iv) The use of monodisperse hard, spherical NMs for intercomparison/validation of analytical techniques of different principles is recommended. In addition, once validated, they can be combined to give additional data such as particle structure (e.g., sphericity and permeability) and an estimate of the thickness of the surface coating of the particles by organic molecules.

■ ASSOCIATED CONTENT

Supporting Information

Synthesis of silver and gold NMs, modeling particle size distribution obtained by AFM, analysis of dynamic light scattering data, AFM images of gold NMs prepared by different methods, AFM images illustrating sample preparation artifacts, AFM images and PSD of NMs studied here, FlFFF calibration curve, and conversion of DLS intensity to volume and number particle size distribution. This material is available free of charge via the Internet at http://pubs.acs.org/.

■ AUTHOR INFORMATION

Corresponding Author

*E-mail: m.a.baalousha@bham.ac.uk; phone: (+44) 121 414 7297; fax: (+44) 1214145528.

Notes

The authors declare no competing financial interest.

■ ACKNOWLEDGMENTS

We acknowledge funding from the UK Natural Environment Research Council (NERC; Grant NE/F005008/1) and the NERC-funded Facility for Environmental Nanoscience Analysis and Characterization.

■ REFERENCES

(1) Global Industry Analysts, Inc. Global Market for Nanotechnology-Enabled Products To Reach US$2.41 Trillion by 2015, According to a New Report by Global Industry Analysts, Inc., 2011. http://www.prweb.com/releases/nanotechnology/nano_products/prweb4719764.htm (accessed April 1, 2012).

(2) Woodrow Wilson Data Base. The Project on Emerging Nanotechnologies, 2012. http://www.nanotechproject.org/ (accessed April 1, 2012).

(3) Christian, P.; Von der Kammer, F.; Baalousha, M.; Hofmann, Th. Nanoparticles: Structure, Properties, Preparation and Behaviour in Environmental Media. *Environ. Toxicol. Chem.* **2008**, *17*, 326−343.

(4) Fabrega, J.; Luoma, S. N.; Tyler, C. R.; Galloway, T. S.; Lead, J. R. Silver Nanoparticles: Behaviour and Effects in the Aquatic Environment. *Environ. Int.* **2011**, *37*, 517−531.

(5) Klaine, S. J.; Alvarez, P. J. J.; Batley, G. E.; Fernandes, T. F.; Handy, R. D.; Lyon, D. Y.; Mahendra, S.; McLaughlin, M. J.; Lead, J. L. Nanomaterials in the Environment: Behaviour, Fate, Bioavailability and Effects. *Environ. Toxicol. Chem.* **2008**, *27*, 1825−1851.

(6) Rivera Gil, P.; Oberdörster, G.; Elder, A.; Puntes, V.; Parak, W. J. Correlating Physico-Chemical with Toxicological Properties of Nanoparticles: The Present and the Future. *ACS Nano* **2010**, *4*, 5527−5531.

(7) Puzyn, T.; Leszczynska, D.; Leszczynski, J. Toward the Development of "Nano-QSAR": Advances and Challenges. *Small* **2009**, *5*, 2494−2509.

(8) Powers, K. W.; Palazuelos, M.; Moudgil, B. M.; Roberts, S. M. Characterization of the Size, Shape, and State of Dispersion of Nanoparticles for Toxicological Studies. *Nanotoxicology* **2007**, *1*, 42−51.

(9) Domingos, R. F.; Baalousha, M.; Ju-Nam, Y.; Reid, M.; Tufenkji, N.; Lead, J. R.; Leppard, G. G.; Wilkinson, K. J. Characterizing Manufactured Nanoparticles in the Environment—Multimethod Determination of Particle Sizes. *Environ. Sci. Technol.* **2009**, *43*, 7277−7284.

(10) MacCuspie, R. I.; Rogers, K.; Patra, M.; Suo, Z.; Allen, A. J.; Martin, M. N.; Hackley, V. A. Challenges for Physical Characterization of Silver Nanoparticles Under Pristine and Environmentally Relevant Conditions. *J. Environ. Monit.* **2011**, *13*, 1212−1226.

(11) Baalousha, M.; Ju-Nam, Y.; Cole, P. A.; Gaiser, B.; Fernandes, T. F.; Hriljac, J. A.; Jepson, M. A.; Stone, V.; Tyler, C. R.; Lead, J. R. Characterization of Cerium Oxide Nanoparticles—Part 1: Size Measurements. *Environ. Toxicol. Chem.* **2012**, *31*, 983−993.

(12) Baalousha, M.; Ju-Nam, Y.; Cole, P. A.; Hriljac, J. A.; Jones, I. P.; Tyler, C. R.; Stone, V.; Fernandes, T. F.; Jepson, M. A.; Lead, J. R. Characterization of Cerium Oxide Nanoparticles—Part 2: Nonsize Measurements. *Environ. Toxicol. Chem.* **2012**, *31*, 994−1003.

(13) Powers, K. W.; Brown, S. C.; Krishna, V. B.; Wasdo, S. C.; Moudgil, B. M.; Roberts, S. M. Research Strategies for Safety Evaluation of Nanomaterials. Part VI. Characterization of Nanoscale Particles for Toxicological Evaluation. *Toxicol. Sci.* **2006**, *90*, 296−303.

(14) Römer, I.; White, T. A.; Baalousha, M.; Chipman, K.; Viant, M. R.; Lead, J. R. Aggregation and Dispersion of Silver Nanoparticles in Exposure Media for Aquatic Toxicity Tests. *J. Chromatogr., A* **2011**, *1218*, 4226−4233.

(15) Baalousha, M.; Lead, J. R. Size Fractionation and Characterization of Natural Aquatic Colloids and Nanoparticles. *Sci. Total Environ.* **2007**, *386*, 93−102.

(16) Gibson, C. T.; Turner, I. J.; Roberts, C. J.; Lead, J. R. Quantifying the Dimensions of Nanoscale Organic Surface Layers in Natural Waters. *Environ. Sci. Technol.* **2007**, *41*, 1339−1344.

(17) Wilkinson, K. J.; Balnois, E.; Leppard, G. G.; Buffle, J. Characteristic Features of the Major Components of Freshwater Colloidal Organic Matter Revealed by Transmission Electron and Atomic Force Microscopy. *Colloids Surf., A* **1999**, *155*, 287−310.

(18) Grobelny, J.; DelRio, F. W.; Pradeep, N.; Kim, D.-I.; Hackley, V. A.; Cook, R. F. NIST-NCL Joint Assay Protocol, PCC-6: Size Measurement of Nanoparticles Using Atomic Force Microscopy, 2009. http://ncl.cancer.gov/NCL_Method_PCC-6.pdf, pp 1−20 (accessed May 14, 2012).

(19) Ungár, T.; Gubicza, J.; Ribárik, G.; Borbély, A. Crystallite Size Distribution and Dislocation Structure Determined by Diffraction Profile Analysis: Principles and Practical Application to Cubic and Hexagonal Crystals. *J. Appl. Toxicol.* **2001**, *34*, 298−310.

(20) Brody, J. P.; Williams, B. A.; Wold, B. J.; Quake, S. R. Significance and Statistical Errors in the Analysis of DNA Microarray Data. *Proc. Natl. Acad. Sci. U.S.A.* **2002**, *99*, 12975−12978.

(21) *ISO22412. Particle Size Analysis—Dynamic Light Scattering (DLS)*; International Organization for Standardization: Geneva, Switzerland, 2008.

(22) Hackley, V. A.; Clogston, J. D. NIST-NCL Joint Assay Protocol, PCC-1: Measuring the Size of Nanoparticles in Aqueous Media Using Batch-Mode Dynamic Light Scattering, 2009. http://ncl.cancer.gov/NCL_Method_PCC-1.pdf (accessed May 14, 2012).

(23) Balnois, E.; Wilkinson, K. J. Sample Preparation Techniques for the Observation of Environmental Biopolymers by Atomic Force Microscopy. *Colloids Surf., A* **2002**, *207*, 229−242.

(24) Baalousha, M.; Motelica-Heino, M.; Galaup, S.; Coustumer, P. Supramolecular Structure of Humic Acids by TEM with Improved

Sample Preparation and Staining. *Microsc. Res. Tech.* **2005**, *66*, 299−306.
(25) Leppard, G. Nanoparticles in the Environment As Revealed by Transmission Electron Microscopy: Detection, Characterisation and Activities. *Curr. Nanosci.* **2008**, *4*, 278−301.
(26) Leppard, G. G.; Burnison, B. K.; Buffle, J. Transmission Electron Microscopy of the Natural Organic Matter of Surface Waters. *Anal. Chim. Acta* **1990**, *232*, 107−121.
(27) Boyd, R. D.; Pichaimuthu, S. K.; Cuenat, A. New Approach to Inter-Technique Comparisons for Nanoparticle Size Measurements; Using Atomic Force Microscopy, Nanoparticle Tracking Analysis and Dynamic Light Scattering. *Colloids Surf., A* **2011**, *387*, 35−42.
(28) Baalousha, M.; Stolpe, B.; Lead, J. R. Flow Field-Flow Fractionation for the Analysis and Characterization of Natural Colloids and Manufactured Nanoparticles in Environmental Systems: A Critical Review. *J. Chromatogr., A* **2011**, *1218*, 4078−4103.
(29) Giddings, C. J.; Stephen Williams, P.; Anna Benincasa, M. Rapid Breakthrough Measurement of Void Volume for Field-Flow Fractionation Channels. *J. Chromatogr., A* **1992**, *627*, 23−35.
(30) Assemi, S.; Newcombe, G.; Hepplewhite, C.; Beckett, R. Characterization of Natural Organic Matter Fractions Separated by Ultrafiltration Using Flow Field-Flow Fractionation. *Water Res.* **2004**, *38*, 1467−1476.
(31) Baalousha, M.; Lead, J. R. Characterization of Natural Aquatic Colloids (<5 nm) by Flow-Field Flow Fractionation and Atomic Force Microscopy. *Environ. Sci. Technol.* **2007**, *41*, 1111−1117.
(32) Baalousha, M.; Manciulea, A.; Cumberland, S.; Kendall, K.; Lead, J. R. Aggregation and Surface Properties of Iron Oxide Nanoparticles; Influence of PH and Natural Organic Matter. *Environ. Toxicol. Chem.* **2008**, *27*, 1875−1882.